# Effect of Polar Solvents on the (2p3s) Rydberg State of Diazabicyclooctane

**Q. Y. Shang,† P. O. Moreno,‡ and E. R. Bernstein***

*Contribution from the Department of Chemistry, Colorado State University, Fort Collins, Colorado 80523*

*Received April 16, 1993. Revised Manuscript Received July 23, 1993®*

**Abstract:** Mass-resolved excitation spectra of the (2p3s) ← $(2p)^2$ Rydberg transition of 1,4-diazabicyclo[2.2.2]octane (DABCO) clustered with polar and nonpolar solvents are reported. The DABCO/solvent clusters are generated in a supersonic expansion. The solvents employed in this study have diverse electronic and dipolar properties and include amines, ethers, aromatics, acetonitrile, a thioether, cyclohexanes, ethylene, $N_2$, and Kr. The spectra can be analyzed in terms of cluster transition origins, van der Waals vibrational modes, and internal DABCO vibrational modes. Potential energy calculations are performed for the cluster ground state using atom–atom potentials. The cluster transition origin shift from that of the isolated DABCO bare molecule is used to characterize the DABCO/solvent interaction in the (2p3s) Rydberg excited state. Blue-shifted transition origins are observed for DABCO/Kr, $N_2$, ethylene, cyclohexane, and methylcyclohexane clusters; these shifts can be interpreted as arising from strong repulsive interactions in the excited Rydberg state between the DABCO 3s electron and the solvent. Red-shifted transition origins are observed for DABCO/amine, ether, aromatic, and acetonitrile clusters. Although significant, the anticipated dipole-induced dipole interaction is not sufficient to explain these substantial red shifts. The large stabilization of the excited Rydberg state in these latter clusters is proposed to arise from a delocalization of the DABCO 3s Rydberg electron into the comparable energy 3s or other orbitals of the solvent; that is, the cluster stabilization is at least partially due to an electron-transfer interaction. This mechanism for enhanced cluster excited-state interaction is especially important for solute/solvent systems with 3s Rydberg orbitals at comparable energies.

## I. Introduction

Cluster spectroscopic studies have contributed a great deal of detailed information concerning both molecular structure and intermolecular interactions.[1-4] Solute/solvent clusters evidence a spectroscopic shift from an isolated solute transition which can be interpreted in terms of the difference between solute and solvent interactions in the ground and excited states. These cluster interactions are found to be highly dependent on specific cluster structure and size. Such data can be employed to unravel complex condensed-phase interactions, which are typically averages of many intermolecular configurations. Extensive results are available on the solvation effects for valence transitions.[1,2] For example, the benzene/argon 1:1 cluster shows a 21-$cm^{-1}$ red shift (a decrease in the transition energy with respect to the bare benzene $\pi$ to $\pi^*$ molecular transition) for the $^1B_{2u} \leftarrow {}^1A_{1g}$ transition.[5] This shift has been interpreted as due to a larger polarizability for benzene in the $^1B_{2u}$ excited $\pi\pi^*$ state than in the ground state. The excited state thereby has a larger cluster binding energy than the ground state.

We have recently begun studying the effect of solvation on transitions to molecular Rydberg states.[6-8] Rydberg states can be long-lived because they are not well coupled to the higher valence states, and they can be quite reactive because the excited electron is in general not tightly bound. A molecular Rydberg state can be loosely defined as an excited electronic state arising from the excitation of a bonding or nonbonding electron to an excited state composed of orbitals of higher principal quantum number than those of the ground state ($n = 2$ to $n = 3$ atomic transitions in this instance). The $n = 3$ atomic orbitals are spatially more extended than the $n = 2$ atomic valence orbitals for C, N, and O. The $n = 3$ Rydberg electronic configuration is thus both diffuse and polarizable. The measured polarizability for the 3s state of some cyclic ketones is a few hundred cubic angstroms:[9] this is more than 2 orders of magnitude larger than the polarizabilities of the ground or valence excited states of these ketones. Although often quite sharp, Rydberg transitions can be readily broadened by the presence of other molecules.[10] The enhanced sensitivity of Rydberg electronic states to nonpolar solvent systems can be related to a repulsive interaction between a closed-shell solvent molecule and the Rydberg electron. This Pauli exclusion interaction changes the intermolecular excited-state potential with respect to that of the ground state.[10,11]

The transition involved in this study is characterized by the general description (2p3s) ← $(2p)^2$ even for systems with two lone pair sites.[6-8,11] As has been pointed out in each specific instance, these states are, of course, more properly described as linear combinations of orbitals from each lone pair atomic site, N or O.

Detailed orientation and position dependent interaction energies for Rydberg state/nonpolar solvent cluster systems have been determined for the (2p3s) ← $(2p)^2$ transitions of dioxane, 1,4-diazabicyclo[2.2.2]octane (DABCO), and azabicyclo[2.2.2]-octane (ABCO).[6-8] Rydberg transitions in these clusters are characterized by a blue shift (larger transition energy) of up to 300 $cm^{-1}$. This shift is a function of both cluster size and structure. Such effects can be modeled by standard atom–atom intermolecular interaction potential energy calculations (Lennard–Jones, exp–6, etc.) for solute and solvent systems in both the ground

† Current address: Applied Materials, Santa Clara, CA.
‡ Current address: Dow Chemical Company, Freeport, Texas.
• Abstract published in *Advance ACS Abstracts,* November 15, 1993.

(1) Bernstein, E. R. *Atomic and Molecular Clusters*; Bernstein, E. R., Ed.; Elsevier: New York, 1990, p 551.
(2) Levy, D. H. *Adv. Chem. Phys.* **1981**, *47*, 323.
(3) Shang, Q. Y.; Bernstein, E. R. *J. Chem. Phys.* **1992**, *97*, 60.
(4) Castella, M.; Tramer, A.; Piuzzi, F. *Chem. Phys. Lett.* **1986**, *129*, 105.
(5) Menapace, J. A.; Bernstein, E. R. *J. Phys. Chem.* **1987**, *91*, 2533.
(6) Moreno, P. O.; Shang, Q. Y.; Bernstein, E. R. *J. Chem. Phys.* **1992**, *97*, 2869.
(7) Shang, Q. Y.; Moreno, P. O.; Li, S.; Bernstein, E. R. *J. Chem. Phys.* **1993**, *98*, 1876.
(8) Shang, Q. Y.; Moreno, P. O.; Dion, C.; Bernstein, E. R. *J. Chem. Phys.* **1993**, *98*, 6769.
(9) Causley, G. C.; Russell, B. R. *J. Chem. Phys.* **1980**, *72*, 2623.
(10) Robin, M. B.; Kuebler, N. A. *J. Mol. Spectrosc.* **1970**, *33*, 274.
(11) Robin, M. B. *Higher Excited States of Polyatomic Molecules*; Academic Press: New York, 1974; Vol. I.

0002-7863/94/1516-0302$04.50/0 

and excited Rydberg states.[8] The results of such analysis show that the blue-shifted transition can be ascribed to an increase in the repulsive part of the potential in the Rydberg state. The repulsive interaction extends to a distance of ~5.0 Å from the 3s Rydberg atomic center (O or N).

Only very limited information is available concerning the effects of polar solvents on molecular Rydberg states. One simple expectation for the polar solvent/molecular Rydberg system is that dipole-induced dipole interactions may become important because of the high polarizability of the Rydberg state. Since the dipole-induced dipole interaction is expected to be small in general for these systems in the ground state, the Rydberg transition energy could be red shifted by polar solvents if the dipole-induced dipole interaction is stronger than the repulsive interaction expected for Rydberg states in nonpolar solvents. The clusters studied in this work will be referred to as solute/solvent clusters and are of the general form DABCO(solvent)$_n$ with $n \geq 1$.

In this paper we report a study of the effect of polar solvents on the (2p3s) Rydberg state of DABCO. This state is generated by the excitation of a 2p lone pair electron centered on the nitrogen atom of DABCO to the 3s orbital. The spectroscopic properties of the DABCO (2p3s) ← $(2p)^2$ Rydberg transition have been discussed and documented in previous publications from this laboratory.[7,8] References to earlier work on this system can be found in these papers. The transition ($A'_1 \leftarrow A'_1$ in $D_{3h}$ symmetry) of the unclustered DABCO is one-photon forbidden and two-photon allowed. Cluster formation reduces the symmetry of the DABCO species to $C_{3v}$ or lower: such a perturbation renders the cluster transition one-photon allowed.

Clusters of most interest to these studies are 1:1 solute (chromophore, DABCO)/solvent systems. These small van der Waals clusters or complexes can be investigated both experimentally and theoretically. Three unique cluster geometries are expected (by calculation) for DABCO(Ar)$_1$ clusters, but only two of these are stable in supersonically generated and cooled clusters.[7] This situation is thoroughly discussed in refs 7 and 8.

The clusters of DABCO with various polar and (for comparison purposes) nonpolar solvents are generated in a supersonic expansion and are accessed for study by two-color mass-resolved excitation spectroscopy (MRES). The polar solvents employed here are $NH_3$, triethylamine (TEA), ABCO, $CH_3OCH_3$, tetrahydropyran (THP), $CH_3CN$, $CH_3SCH_3$, methylcyclohexane, and toluene. The nonpolar solvents employed are DABCO, dioxane, benzene, ethylene, $N_2$, cyclohexane, and Kr. Results of these comparisons suggest that dipole-induced dipole interactions have a significant influence on the highly polarizable Rydberg state. Nonetheless, this interaction cannot alone account for the observed large red shifts of the cluster Rydberg transition for solvents such as amines, ethers, and aromatics. A new model interaction is put forward in which the solute 3s Rydberg electron is delocalized into the comparable Rydberg orbital of the solvent. This interaction is in essence an intermolecular charge- or electron-transfer interaction between the solute and solvent molecules of the cluster.

## II. Procedures

**A. Experiments.** Our supersonic expansion and mass-resolved excitation apparatus has been previously described.[6,12] Only a few details specific to the results presented in this paper will be discussed here. DABCO is placed in the head of a Jordan pulsed nozzle in a glass boat. The sample tempertaure is controlled between 25 and 50 °C to adjust cluster signal levels for a particular cluster system. The expansion backing pressure is typically set to 50 psig, and the expansion gas is helium. Individual solvent gases are premixed with the expansion gas at about 0.5–5.0% (pressure) concentration to adjust for appropriate signal levels. Clusters formed under these expansion conditions typically have a translational temperature of ca. 0.1 K, a rotational temperature of ca. 3–5 K, and a vibrational temperature of ca. 10–50 K.[1]

Spectra are taken with a Nd:YAG pumped dye laser with ultraviolet wavelengths generated by doubling and mixing crystals. Three dyes, R590 doubled (35 100–36 000 cm$^{-1}$), F548 doubled (35 800–36 800 cm$^{-1}$), and LDS 750 doubled and mixed with a 1.064-μm Nd:YAG fundamental (36 750–37 700 cm$^{-1}$), are employed to cover the required wavelength range for the DABCO cluster spectra. Each cluster system is investigated over a wide range of energies to search for cluster origins and vibrational modes: this typically covers the range from 600 cm$^{-1}$ below the bare molecule (two-photon allowed) transition origin to 1000 cm$^{-1}$ above it.

To ensure that the spectra reported are only related to the DABCO-(solvent)$_1$ cluster, two-color threshold ionization is employed for all systems. The ionization laser is also a Nd:YAG-pumped dye laser, employing third-harmonic dye pumping and coumarin 460 dye (ionization wavelength ca. 450 nm). Additionally, the DABCO(solvent)$_2$ cluster channel is monitored when appropriate to look for spectral overlaps and possible fragmentation into the lower mass channel.

**B. Calculations.** The methods used for the DABCO/solvent cluster geometry calculations are described previously.[8] Potential functions and parameters are obtained from ref 13. The geometry of the molecule and its atomic partial charges are obtained from MOPAC 6 (AM1) calculations.[14]

## III. Results

**A. Calculated Cluster Geometry.** Calculation of the cluster minimum energy geometries, employing a Lennard–Jones–Coulomb atom–atom potential energy function, for DABCO clustered with dimethyl ether, benzene, dioxane, ammonia, DABCO, and others, generates a number of different stable local minimum energy structures for each cluster system. These various structures can in general be categorized into three structural groups, as presented previously for DABCO(Ar)$_1$.[7] Within each of these three groups (sites I, II, III, as described in ref 7), solvent orientational preferences can create additional cluster structures. The most stable geometry, however, is always one for which the solvent is located over the nitrogen end of the DABCO molecule. Figure 1 displays this particular lowest energy cluster conformation for a number of DABCO(solvent)$_1$ clusters. The binding energies listed in Figure 1 are the largest calculated for each cluster: other cluster geometries have binding energies at least 100–200 cm$^{-1}$ less than those for the respective DABCO(solvent)$_1$ clusters. Specific spectroscopic features are assigned to these calculated cluster structures in our previously reported studies.[7,8] These assignments are completely consistent with the results reported in this work and will be assumed to be correct in the ensuing discussion.

The results presented below suggest that most of the clusters are present in the expansions in a single conformation. We assume that this cluster geometry is the most stable calculated one, as presented in Figure 1.

**B. MRES of DABCO/Amine Clusters.** Figure 2 presents the MRES of DABCO$(NH_3)_1$, $((C_2H_5)_3N)_1$, (ABCO)$_1$, and (DABCO)$_1$. These spectra are displayed in a region to the red of the DABCO bare molecule origin (35 786.0 cm$^{-1}$)[7] for the (2p3s) ← $(2p)^2$ Rydberg transition. The region to the blue of the DABCO Rydberg $0_0^0$ transition shows no new cluster origins. Peak assignments and positions are given in Table I. These assignments are made on the basis of cluster transition origins, van der Waals vibrational modes, and internal vibrations of the DABCO molecule.

The spectrum of DABCO$(NH_3)_1$ is very broad: its onset is at ca. 35 650 cm$^{-1}$. This onset is red shifted from the DABCO bare molecule origin by more than 150 cm$^{-1}$. The spectrum extends continuously to beyond $0_0^0$ + 1000 cm$^{-1}$.

The spectrum of DABCO(TEA)$_1$ in Figure 2 is well resolved. The most intense and most red-shifted spectral feature for this cluster is at 35 364 cm$^{-1}$; this feature is assigned as the (2p3s) Rydberg state transition origin of the DABCO(TEA)$_1$ most stable

(12) Berstein, E. R.; Law, K.; Schauer, M. *J. Chem. Phys.* **1984**, *80*, 207.

(13) Nemethy, G.; Pottle, M. S.; Scheraga, H. A. *J. Phys. Chem.* **1983**, *87*, 1883.

(14) Stewart, J. J. P. *A General Molecular Orbital Package MOPAC*, 6th ed.; QCPE 455, 1989.

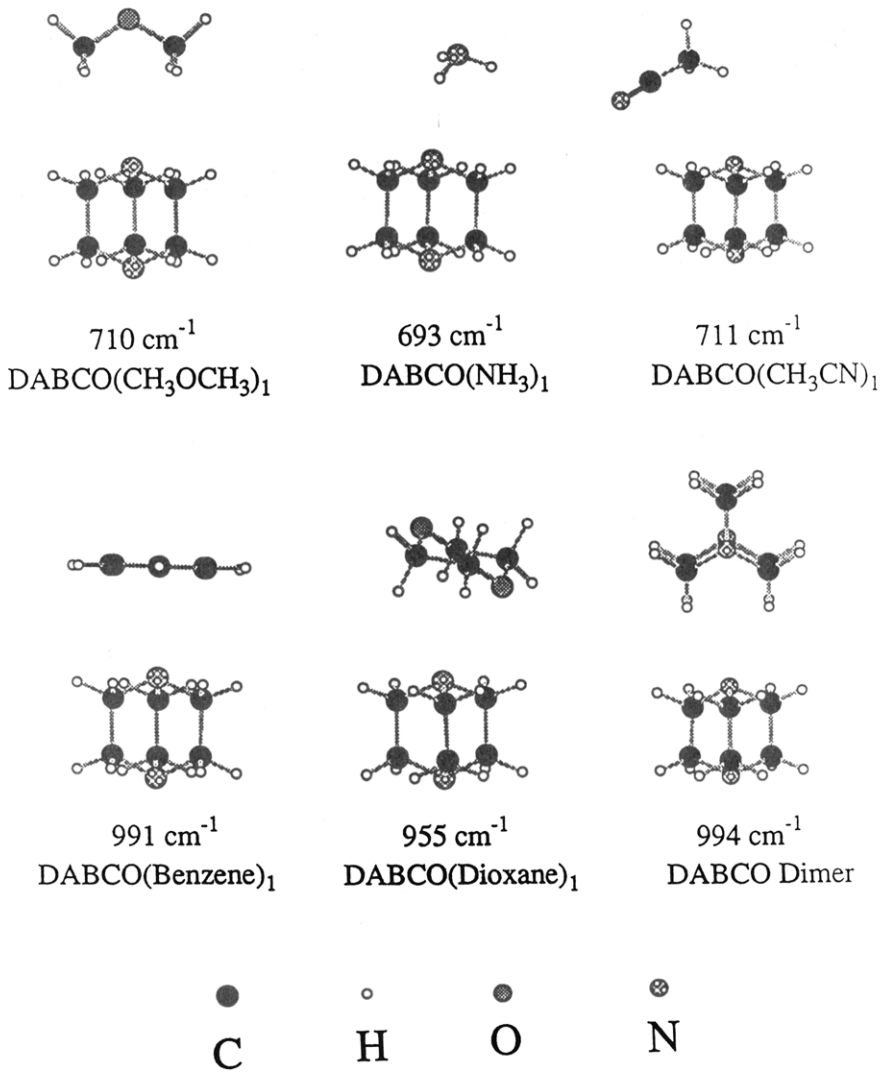


**Figure 1.** Most stable geometry and binding energy of the 1:1 DABCO/solvent cluster calculated from a 6-12-1 potential. Solvents are methyl ether, ammonia, acetonitrile, DABCO (dimer), dioxane, and benzene.

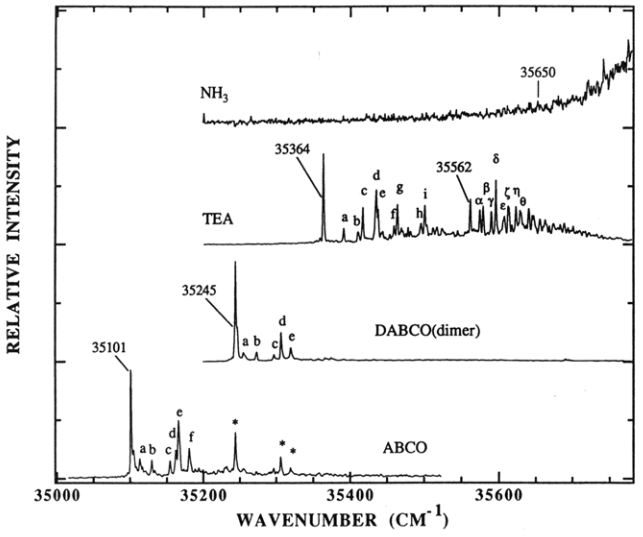


**Figure 2.** Two-color one-photon resonance MRES of the 1:1 DABCO/amine clusters. The right-hand frame marks the two-photon origin energy for the DABCO bare molecule (35 786 $cm^{-1}$). Peaks labeled by • are from the DABCO dimer mass channel. Detailed peak positions and assignments are given in Table I.

cluster. Many features are built on this origin. In order to determine whether some of these features might arise from a cluster of the same composition but different equilibrium geometry, "population depletion/hole-burning" experiments are performed on this system.[3] The peaks at 35 364 and 35 562 $cm^{-1}$ are employed for the probe laser position. These experiments demonstrate that transitions to the red of 35 562 $cm^{-1}$ belong to one cluster and that the feature at 35 562 $cm^{-1}$ (assumed to be an origin) and features to the blue of it belong to a cluster having the same composition but a different geometry. Since more than six peaks follow each origin within ca. 150 $cm^{-1}$, one can conclude that van der Waals modes and their combinations and overtones are observed in these cluster spectra. Moreover, none of the observed energy spacings appears in both sets of spectra, so molecular vibrations are not observed in this instance.

Also shown in Figure 2 is the spectrum of the DABCO dimer. The origin transition is most intense and red shifted by more than 500 $cm^{-1}$. Features following the origin are clearly transitions involving van der Waals modes. These spectra arise from a single $(DABCO)_2$ geometry. None of the observed features can be attributed to exciton or resonance interactions.

The origin of the $DABCO(ABCO)_1$ cluster spectrum (Figure 2) lies at 35 101 $cm^{-1}$, red shifted from the DABCO bare molecule origin by 685 $cm^{-1}$. At least six weak features can be identified as being built on this origin; they are assigned as being due to transitions involving van der Waals modes in the cluster (2p3s) Rydberg state. Again, only one major cluster geometry can be identified in this spectrum.

Note that all the $DABCO(amine)_1$ clusters show a substantial spectral red shift with respect to the bare DABCO molecule origin. The size of this shift does not correlate with solvent dipole moment. This point will be treated at some length in the Discussion section.

**Table I.** Transition Energies and Assignments of DABCO/Solvent Cluster Spectra

| cluster DABCO/solvent | transition energy ($cm^{-1}$) | relative energy ($cm^{-1}$) origin shift | relative energy ($cm^{-1}$) vibration | label, assignment[a] | cluster DABCO/solvent | transition energy ($cm^{-1}$) | relative energy ($cm^{-1}$) origin shift | relative energy ($cm^{-1}$) vibration | label, assignment[a] |
|---|---|---|---|---|---|---|---|---|---|
| DABCO bare molecule | 35 786 | 0.0 | | two-photon origin, (2p3s) ← (2p)$^2$ | | 35 578 | | 67 | c′ (a′ + b′), vdW |
| $NH_3$ | 35 650 | −136 | | origin, broad | | 35 593 | | 82 | d′ (2 × b′), vdW |
| TEA | 35 364 | −422 | | origin I | | 35 618 | | 107 | e′ (a′ + 2 × b′), vdW |
| | 35 392 | | 28 | a, vdW | | 35 634 | | 123 | f′ (3 × b′), vdW |
| | 35 411 | | 47 | b, vdW | | 35 656 | | 145 | g′ (a′ + 3b′), vdW |
| | 35 417 | | 53 | c, vdW | | 35 673 | | 162 | h′ (4 × b′), vdW |
| | 35 436 | | 72 | d, vdW | | 35 694 | | 183 | i′ (a′ + 4 × b′), vdW |
| | 35 438 | | 74 | e, vdW | | 35 715 | | 204 | j′ (5 × b′), vdW |
| | 35 460 | | 96 | f, vdW | | 35 733 | | 222 | k′ (a′ + 5 × b′), vdW |
| | 35 464 | | 100 | g, vdW | | 35 751 | | 240 | l′ (6 × b′), vdW |
| | 35 496 | | 132 | h, vdW | cyclohexane | 36 130 | 344 | | origin |
| | 35 501 | | 137 | i, vdW | | 36 168 | | 38 | a, vdW |
| | 35 562 | −224 | | origin II | | 36 171 | | 41 | b, vdW |
| | 35 575 | | 13 | α, vdW | | 36 207 | | 77 | c, vdW |
| | 35 579 | | 17 | β, vdW | | 36 332 | | 202 | A, iv |
| | 35 590 | | 28 | γ, vdW | | 36 578 | | 448 | B, iv |
| | 35 596 | | 34 | δ, vdW | methylcyclohexane | 36 181 | 358 | | origin |
| | 35 606 | | 44 | ε, vdW | | 36 134 | | −47 | b′, hot band |
| | 35 608 | | 46 | ζ, vdW | | 36 172 | | −9 | a′, hot band |
| | 35 613 | | 51 | η, vdW | | 36 188 | | 7 | a, vdW |
| | 35 624 | | 62 | θ, vdW | | 36,195 | | 14 | b, vdW |
| DABCO dimer | 35 245 | −541 | | origin | | 36 207 | | 26 | c, vdW |
| | 35 257 | | 12 | a, vdW | | 36 221 | | 40 | d, vdW |
| | 35 274 | | 29 | b, vdW | | 36 385 | | 204 | A, iv |
| | 35 297 | | 52 | c, vdW | $C_6H_6$ | 35 452 | −334 | | origin |
| | 35 308 | | 63 | d, vdW | | 35 458 | | 6 | a, vdW |
| | 35 320 | | 75 | e, vdW | | 35 461 | | 9 | b (2 × a), vdW |
| ABCO | 35 101 | −685 | | origin | | 35 465 | | 13 | c (3 × a), vdW |
| | 35 113 | | 12 | a, vdW | | 35 523 | | 71 | d, vdW |
| | 35 129 | | 28 | b, vdW | | 35 583 | | 131 | e (2 × d), vdW |
| | 35 153 | | 52 | c, vdW | toluene | 35 422 | −364 | | origin |
| | 35 161 | | 60 | d, vdW | | 35 437 | | 15 | a, vdW |
| | 35 165 | | 64 | e, vdW | | 35 451 | | 29 | b, vdW |
| | 35 181 | | 80 | f, vdW | | 35 482 | | 60 | c, vdW |
| 1,4-dioxane | 35 600 | −186 | | origin, broad | | 35 487 | | 65 | d, vdW |
| $CH_3OCH_3$ | 35 327 | | −4 | hot band | | 35 523 | | 101 | e, vdW |
| | 35 331 | −455 | | origin I | | 35 547 | | 125 | f, vdW |
| | 35 400 | | 69 | a, vdW | $CH_3SCH_3$ | 35 858 | 72 | | origin |
| | 35 413 | | 82 | b, vdW | | 35 883 | | 25 | a, vdW |
| | 35 424 | | 93 | c, vdW | | 35 890 | | 32 | b, vdW |
| THP | 35 233 | −553 | | origin I | | 35 915 | | 57 | c, vdW |
| | 35 252 | | 19 | a, vdW | | 35 940 | | 82 | d, vdW |
| | 35 271 | | 38 | b (2 × a), vdW | | 35 950 | | 92 | e, vdW |
| | 35 290 | | 57 | c (3 × a), vdW | | 35 963 | | 105 | f, vdW |
| | 35 303 | | 70 | d, vdW | | 35 972 | | 114 | g, vdW |
| | 35 309 | | 76 | e (4 × a), vdW | | 35 980 | | 122 | h, vdW |
| | 35,313 | | 80 | f, vdW | | 36 027 | | 169 | i, vdW |
| | 35 322 | | 89 | g (d + a), vdW | | 36 038 | | 180 | j, vdW |
| | 35 325 | | 92 | h, vdW | | 36 048 | | 190 | k, vdW |
| | 35 331 | | 98 | i (f + a), vdW | | 36 066 | | 208 | l, vdW |
| | 35 340 | | 107 | j (d + 2a), vdW | $CH_3CN$ | 35 200 | −586 | | broad origin |
| | 35 350 | | 117 | k (f + 2a), vdW | Kr | 35 882 | 96 | | origin I |
| | 35 358 | | 125 | l (d + 3a), vdW | | 36 329 | | 447 | B, iv |
| | 35 377 | | 144 | m (f + 3a), vdW | | 36 075 | 289 | | origin II |
| | 35 511 | −275 | | origin II | $N_2$ | 36 055 | 269 | | origin |
| | 35 536 | | 25 | a′, vdW | | 36 260 | 474 | | DABCO$(N_2)_2$ |
| | 35 552 | | 41 | b′, vdW | $C_2H_4$ | 35 983 | 197 | | origin |

[a] iv, internal vibration of DABCO; vdW, intermolecular van der Waals vibration.

**C. MRES of DABCO/Ether Clusters.** Figure 3 presents the spectra of DABCO$(CH_3OCH_3)_1$, $(THP)_1$, and $(dioxane)_1$ clusters. Conditions for these experiments are similar to those used for the amine studies. Note that all these origins are again red shifted.

The spectrum of DABCO$(dioxane)_1$ is very broad. Most of the sharp structure superimposed on this background is noise. The width of this spectrum is roughly 350 $cm^{-1}$. This width is probably associated with both multiple cluster geometries and long Franck–Condon progressions involving cluster modes.

The DABCO$(CH_3OCH_3)_1$ cluster spectrum (Figure 3) is composed of a number of sharp features, the lowest energy of which are at 35 327 and 35 331 $cm^{-1}$. These features are not due to a single species with a common ground state on the basis of population depletion/hole-burning studies. Additionally, the lowest energy transition at 35 327 $cm^{-1}$ serves as an origin for features a, b, and c. Thus, either the peaks 35 327 $cm^{-1}$, a, b, and c are all hot bands from the same ground-state mode or 35 327 $cm^{-1}$ is an origin of one cluster geometry with a, b, and c built on it and 35 331 $cm^{-1}$ is a hot band or another origin. On the basis of population depletion/hole-burning studies, we conclude that the other features in the spectrum are due to clusters of the same composition but different geometries. The crowding of peaks to higher energy makes hole-burning experiments difficult to carry out in a definitive fashion.

The results and conclusions drawn from these hole-burning experiments can in principle be complicated by fragmentation of larger solute(solvent)$_n$ clusters. The fragmentation can occur from either the intermediate ($S_1$) state or the final ion ground electronic state, depending upon which laser places sufficient excess (more than the cluster-binding energy in that electronic state) vibrational energy into the cluster to break the solute–

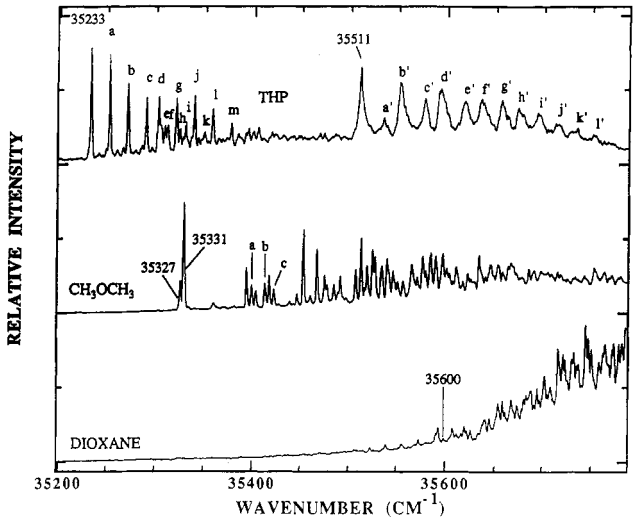


**Figure 3.** Two-color one-photon resonance MRES of the 1:1 DABCO/ether clusters. The right-hand frame marks the two-photon origin energy for the DABCO bare molecule. Detailed peak positions and assignments are given in Table I.

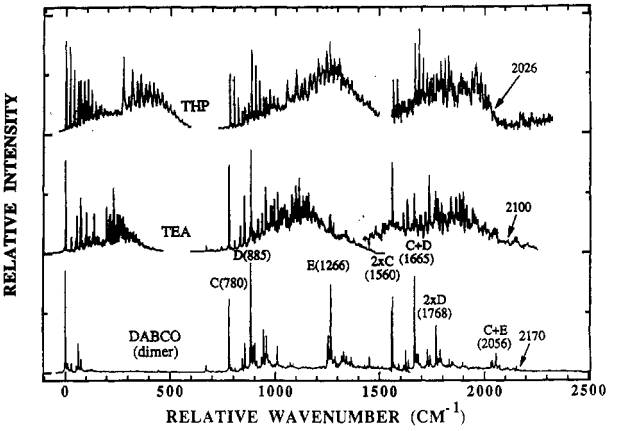


**Figure 4.** Two-color one-photon resonance MRES of the DABCO dimer, DABCO(TEA)$_1$, and DABCO(THP)$_1$. The spectra are plotted in relative energy with respect to the origin transitions of the clusters. (See Figures 2 and 3.) The labeled peaks can be assigned as the internal modes of the bare molecule. The arrows mark the cluster dissociation energy.

solvent bond. Both possible cluster fragmentation sources can be eliminated by carefully adjusting the laser energies and their relative arrival times in a two-color MRES experiment. The cluster intermediate state can be excited such that its vibrational energy is kept below the cluster-binding energy or such that its time for fragmentation can be measured.[6-8] The cluster can also be ionized near the ionization threshold energy.[6-8]

The DABCO(THP)$_1$ cluster spectrum (Figure 3) clearly displays features belonging to two distinct cluster geometries. The origin of the first cluster structure is at 35 233 $cm^{-1}$. The peaks labeled a–m following this $0_0^0$ transition are assigned to transitions involving cluster van der Waals modes in the excited (2p3s) Rydberg state. The origin of the second cluster structure is at 35 511 $cm^{-1}$, and it is followed by a long progression in a 40-$cm^{-1}$ van der Waals mode (a′–l′). The features associated with the higher energy cluster transition are quite broad (ca. 10 $cm^{-1}$ vs 3 $cm^{-1}$ for the lower energy cluster transition). This width could arise from unresolved structure due to internal rotational motion in the cluster of this particular structure, and/or it could be associated with dynamical behavior. Peak assignments and positions are given in Table I.

The red shifts observed for these DABCO/ether clusters do not scale with solvent dipole moment, although some of the observed shifts could be partially due to solvent dipole moment.

**D. Internal DABCO Vibrational Modes in Cluster Spectra.** Figure 4 displays the complete cluster spectra for three representative clusters: (DABCO)$_2$, DABCO(TEA)$_1$, and DABCO(THP)$_1$. These spectra are sharp and vary in the extent to which van der Waals modes contribute to their intensity. The DABCO dimer shows most of its intensity in the origin and molecular vibrational modes. The vibrational mode features are labeled C, D, and E in the figure; various combinations and overtones are also labeled as appropriate. All these features are present in the two-photon-allowed bare molecule spectrum and thus verify the cluster origin assignment of the $0_0^0$ (2p3s) Rydberg transition.[15] All these features have the same cluster/bare molecule shift as does the origin (ca. −540 $cm^{-1}$). One can additionally see from Figure 4 that DABCO(TEA)$_1$ and DABCO(THP)$_1$ clusters have comparable features at the same shift values. Spectra of these two latter clusters appear more complicated than those of (DABCO)$_2$ because of additional cluster geometries and substantial van der Waals mode transition intensity. Note too that the spectral shift similarity (see Table I) for the three clusters displayed in Figure 4 indicates that the shift of the DABCO dimer has little or no contribution from excitation or resonance exchange interactions.[16]

The DABCO dimer spectrum becomes quite weak and broad at energies above 2000 $cm^{-1}$ (C + E transition). One can also expect to observe such features as D + E (2152 $cm^{-1}$) as well as higher energy transitions. Such features are observed in the bare molecule spectrum. Loss of the (DABCO)$_2$ spectrum at ca. 2170 $cm^{-1}$ can only be understood in terms of cluster dissociation. Due to the breadth and intensity of the (DABCO)$_2$ spectrum above $0_0^0$ + 2000 $cm^{-1}$, we are unable to make a definitive observation of dimer decomposition in the monomer mass channel. The cluster signal should disappear if the cluster dissociates in times shorter than ca. 1 ns. According to RRKM theory for cluster dissociation,[17] a cluster will dissociate in this time with ca. 2200 $cm^{-1}$ of total energy if its binding energy is ca. 1750 $cm^{-1}$. The cluster requires above 450 $cm^{-1}$ of excess vibrational energy in order for the dissociation to be noticed in the MRES. The most stable (DABCO)$_2$ structure is given in Figure 1, and its calculated binding energy is 950 $cm^{-1}$. Thus, the estimated excited-state binding energy is ca. 1500 $cm^{-1}$ (=950 + 540 $cm^{-1}$). This "calculated" value compares favorably with the above "experimental" value. Similar binding energy estimates can be made for DABCO(TEA)$_1$ and (THP)$_1$ clusters. Their calculated ground-state binding energies are similar to that of the DABCO dimer.

**E. MRES of DABCO/Cyclic Hydrocarbon Clusters.** Figure 5 displays the two-color MRES of DABCO(cyclohexane)$_1$, (methylcyclohexane)$_1$, (benzene)$_1$, and (toluene)$_1$ clusters. The spectra of DABCO(cyclohexane)$_1$ and (methylcyclohexane)$_1$ resemble those of DABCO($C_nH_{2n+2}$)$_1$ clusters.[8] They are characterized by large (>300 $cm^{-1}$) blue shifts and short Franck–Condon progressions in a few van der Waals modes. The transition origin for DABCO($C_6H_{12}$)$_1$ is assigned at 36 130 $cm^{-1}$, the first intense feature of the spectrum. Its blue shift from the DABCO bare molecule origin is 344 $cm^{-1}$. In this spectrum, a, b, and c are transitions involving excited-state van der Waals modes and A and B label internal modes of DABCO. The DABCO(methylcyclohexane)$_1$ transition origin is at 36 181 $cm^{-1}$, 358 $cm^{-1}$ blue shifted from the DABCO bare molecule origin. Peaks b′ and a′ could be due either to hot bands or to a cluster of a different conformation. Peaks a, b, and c can be identified as due to transitions including excited-state van der Waals modes, and

(15) Gonohe, N.; Yatsuda, N.; Mikami, N.; Ito, M. *Bull. Chem. Soc. Jpn.* **1982**, *55*, 2796.

(16) Law, K.; Schauer, M.; Bernstein, E. R. *J. Chem. Phys.* **1984**, *81*, 4871.

(17) (a) Hineman, M. F.; Kim, S. K.; Bernstein, E. R.; Kelley, D. F. *J. Chem. Phys.* **1992**, *96*, 4904. (b) Hineman, M.; Bernstein, E. R.; Kelley, D. F. *J. Chem. Phys.* **1993**, *98*, 2516. (c) Nimlos, M. R.; Young, M. A.; Bernstein, E. R.; Kelley, D. F. *J. Chem. Phys.* **1989**, *91*, 5268 and references to earlier work cited therein. (d) Outhouse, E. A.; Bickel, G. A.; Dremmer, D. R.; Wallace, S. C. *J. Chem. Phys.* **1991**, *95*, 6261.

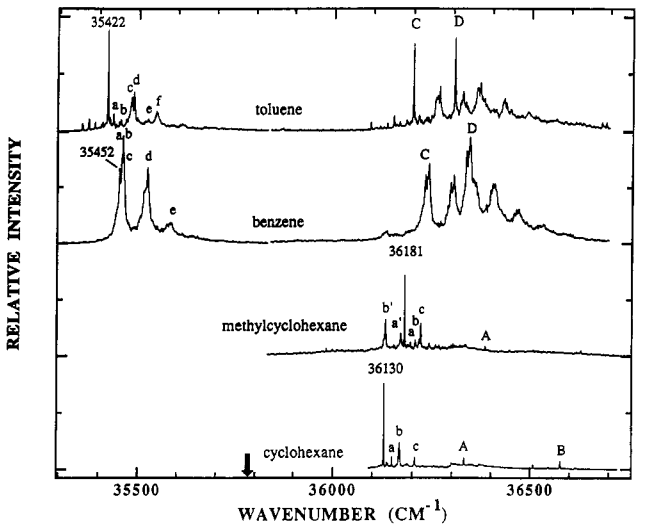


**Figure 5.** Two-color one-photon resonance MRES of the 1:1 DABCO/cyclic hydrocarbon clusters. The arrow marks the two-photon origin energy for the bare molecule. Detailed peak positions and assignments are given in Table I.

feature A is due to a vibronic transition involving an internal mode of DABCO. The data and assignments are collected in Table I.

The DABCO/aromatic hydrocarbon spectra are very different from those of the saturated cyclic or linear hydrocarbons. The DABCO(benzene)$_1$ and (toluene)$_1$ cluster spectra are also presented in Figure 5. The origins of both these clusters are shifted to lower energy than the DABCO bare molecule origin. The origin of the DABCO(benzene)$_1$ cluster Rydberg transition lies at 35 452 cm$^{-1}$. This feature is red shifted by 334 cm$^{-1}$. The features d and e of this spectrum are clearly due to transitions to excited-state van der Waals vibrations. The origin features (35 452 cm$^{-1}$ and a, b, c) may be partially due to internal rotational transitions (in both the ground and excited electronic states) of the benzene molecule with respect to DABCO. Additionally, a new set of features appears at ca. 36 200 cm$^{-1}$ (C, D), associated with internal modes of DABCO: similar features arise for amine and other clusters of DABCO (Figure 4). The entire observed DABCO(benzene)$_1$ cluster spectrum appears to be associated with just one cluster geometry. The spectrum of the DABCO-(toluene)$_1$ cluster can be similarly assigned. The origin at 35 422 cm$^{-1}$ is probably sharper than that of the benzene cluster because of a more restrictive rotational potential for toluene with respect to DABCO. Both ground- and excited-state van der Waals modes are observed about this origin. Features at ca. 36 200 cm$^{-1}$ (C, D) are again assigned to transitions involving internal DABCO vibrations and their van der Waals additions.

**F. MRES of DABCO/$CH_3SCH_3$ and $CH_3CN$ Clusters.** Figures 6 and 7 display the two-color MRES of DABCO($CH_3SCH_3$)$_1$ and ($CH_3CN$)$_1$ clusters. The first peak in the $CH_3SCH_3$ cluster spectrum is at 35 858 cm$^{-1}$ and is assigned as the cluster Rydberg transition origin. It is blue shifted from the bare molecule DABCO Rydberg-state transition origin by 72 cm$^{-1}$. Van der Waals additions to this feature are assigned as features a–l on the figure. Feature C (+780 cm$^{-1}$ from 35 858 cm$^{-1}$) is a transition to a DABCO internal mode. The feature at 36 530 cm$^{-1}$ is probably due to another cluster conformation: it is followed by at least three van der Waals mode additions.

Figure 7 displays the broad featureless spectrum of the DABCO($CH_3CN$)$_1$ cluster. The onset of the (2p3s) Rydberg transition for this cluster is at approximately 35 200 cm$^{-1}$. Both $CH_3CN$ and $CH_3SCH_3$ are polar molecules, but their electronic structures are quite different from those of the ether and amine solvents discussed above. The shifts found for DABCO/$CH_3CN$ and $CH_3SCH_3$ clusters will be analyzed in the Discussion section. These data and assignments are collected in Table I.

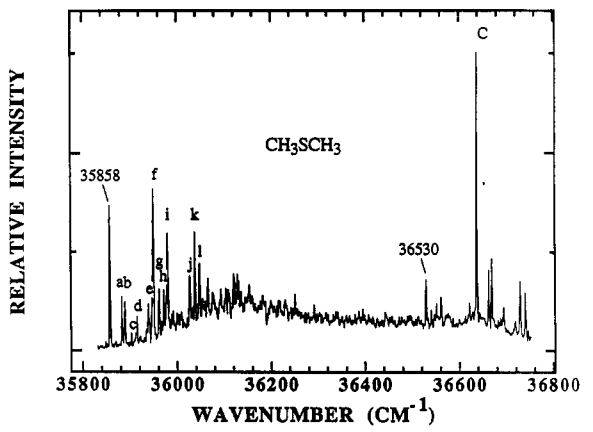


**Figure 6.** Two-color one-photon resonance MRES of DABCO($CH_3SCH_3$)$_1$. The left-hand frame marks the origin energy for the bare molecule. Detailed peak positions and assignments are given in Table I.

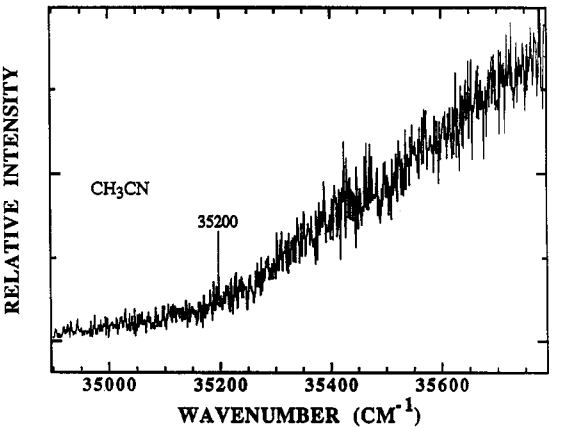


**Figure 7.** Two-color one-photon resonance MRES of DABCO($CH_3CN$)$_1$. The right-hand frame marks the two-photon origin energy for the bare molecule.

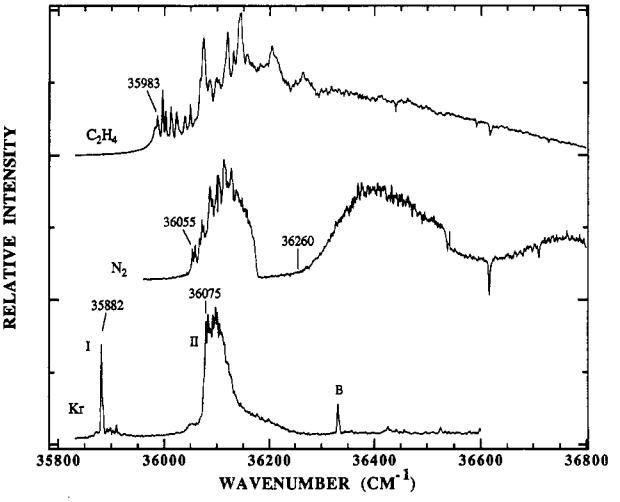


**Figure 8.** Two-color one-photon resonance MRES of the 1:1 DABCO/nonpolar solvent clusters. The left-hand frame marks the two-photon origin energy for the bare molecule. Detailed peak positions and assignments are given in Table I.

**G. MRES of DABCO/Kr, $N_2$, and $C_2H_4$ Clusters.** Figure 8 presents the MRES of DABCO(Kr)$_1$, ($N_2$)$_1$, and ($C_2H_4$)$_1$. The spectrum of DABCO(Kr)$_1$ is similar to that of DABCO(Ar)$_1$.[7] Cluster calculations show the same behavior with regard to both structure and binding energies. The binding energies of the Kr clusters are appropriately larger than those of the Ar clusters, however. The first sharp peak of the DABCO(Kr)$_1$ cluster spectrum at 35 882 cm$^{-1}$ can be assigned as the origin transition for the cluster geometry with Kr centered between two adjacent

DABCO C–C bonds.[7] A few low-intensity van der Waals transitions are observed to the high-energy side of the origin. Another, broad feature for the Kr cluster begins at 36 075 $cm^{-1}$. This latter feature correlates to one assigned for the DABCO-$(Ar)_1$ cluster in which Ar is coordinated to the nitrogen end of the DABCO molecule. For the Ar cluster this geometry is dissociative at ca. 20 $cm^{-1}$ above the onset of the transition. The DABCO$(Kr)_1$ cluster does not obviously dissociate at this transition; this is a result of the increased binding energy for DABCO/Kr with respect to DABCO/Ar. The sharp feature labeled B in Figure 8 is due to an internal vibrational mode of DABCO.

The spectrum of DABCO$(N_2)_1$ shows two prominent broad features. The lower energy feature begins near 36 055 $cm^{-1}$ and has a number of sharp peaks built on it which are presumably van der Waals additions (both rotations[18] and vibrations) to the origin transition. The onset of this broad feature is nearly 269 $cm^{-1}$ blue of the bare DABCO origin. At 36 177 $cm^{-1}$ this broad feature abruptly terminates; similar behavior has been recorded for DABCO$(Ar)_1$ features and has been attributed to dissociation of the cluster. This suggests that the DABCO$(N_2)_1$ excited-state binding energy is ~122 $cm^{-1}$. The cluster experimental binding energy in the ground state is then roughly 391 $cm^{-1}$. The calculated ground-state binding energy for the most stable cluster is 380 $cm^{-1}$.

The second broad feature in this spectrum begins at ca. 36 260 $cm^{-1}$ and ends abruptly near 36 540 $cm^{-1}$. This shift and dissociation limit suggest that this feature belongs to a DABCO/$N_2$ cluster of another geometry. On the basis of these data the cluster would have a ground-state binding energy of ~760 $cm^{-1}$. This large binding energy is inconsistent with that of other clusters and with calculations. This DABCO$(N_2)_1$ signal probably arises from dissociation of a DABCO$(N_2)_2$ cluster: comparable behavior is assigned for the DABCO/Ar cluster system.[7]

The DABCO$(C_2H_4)_1$ cluster system is rich in both sharp and broad features. The first feature in the spectrum lies at 35 983 $cm^{-1}$. The origin of the spectrum may well be one of the other nearby features. The sharp peaks in this spectrum arise from a combination of transitions to excited-state van der Waals modes and multiple geometries.

In general, the spectra of DABCO$(Kr)_1$, $(N_2)_1$, and $(C_2H_4)_1$ clusters all show large blue shifts from the DABCO bare molecule spectrum. Similar blue shifts are characterized for DABCO-$(Ar)_n$ and $(C_nH_{2n+2})_m$ cluster spectra.[8] This observation is consistent with an enhanced repulsive interaction between the DABCO (2p3s) Rydberg state and nonpolar solvents. These data and assignments are collected in Table I.

## IV. Discussion

The difference between the cluster transition energy and that of the bare molecule is referred to as the transition energy cluster shift. This shift can be employed to yield the binding energy difference between the ground and excited (Rydberg) states of the cluster under the conditions that the cluster structure is similar in both electronic states and that the solute geometry is similar in the cluster and the bare molecule. The spectra presented in the figures generally show both of these assumptions to be valid; the major intensity in the observed Rydberg transitions falls at the molecular features, and the relative intenities of the molecular features are similar in the cluster and bare molecule spectra. On the basis of these results, the cluster transition shift is equated to the difference in cluster-binding energy for the ground and Rydberg excited states. Table II contains a compilation of the transition energy shifts for the major (most intense) cluster geometries for all the clusters identified. The dipole moment, the polarizability, and the dipole-induced dipole interaction for each solvent are also presented in this table. A large blue shift (greater than $10^2$ $cm^{-1}$) is observed for DABCO clustered with the nonpolar solvents Kr, $N_2$, $C_2H_4$, and $C_6H_{12}$. DABCO clustered with the slightly polar methylcyclohexane still evidences a large blue shift. The DABCO/$CH_3SCH_3$ cluster has a blue shift of ~70 $cm^{-1}$ even though the dipole moment of the solvent is quite large (1.5 D). Very large red shifts are observed for DABCO/amine, ether, and aromatic solvent clusters. Apparently, a simple correlation between cluster shift and solvent dipole moment is not observed, and thus the dipole-induced dipole interaction cannot alone be responsible for the changes in cluster-binding energy upon electronic excitation to the Rydberg state.

**Table II.** Transition Origin Shift of the Major Cluster Geometry of DABCO(Solvent)$_1$, Solvent Dipole Moment,[20] Polarizability,[20] and the Calculated Maxmium Dipole-Induced Dipole Interaction Energy from Eq 2 in the Text

| solvent molecule | transition origin shift ($cm^{-1}$) | dipole moment (D) | dipole-induced dipole interaction energy ($cm^{-1}$) | solvent polarizability ($Å^3$) |
|---|---|---|---|---|
| Kr | 96 | 0 | 0 | 2.5 |
| $N_2$ | 269 | 0 | 0 | 1.7 |
| $C_2H_4$ | 197 | 0 | 0 | 4.2 |
| cyclohexane | 344 | 0 | 0 | 11.0 |
| methyl cyclohexane | 358 | | | |
| benzene | −334 | 0 | 0 | 10.3 |
| dioxane | −186 | 0 | 0 | 10.0 |
| DABCO | −541 | 0 | 0 | |
| toluene | −364 | 0.36 | −166 | 12.3 |
| TEA | −422 | 0.66 | −491 | 13.1 |
| ABCO | −685 | 1.2[a] | −184 | |
| $CH_3OCH_3$ | −455 | 1.3 | −216 | 5.2 |
| $NH_3$ | −136 | 1.47 | −243 | 2.3 |
| $CH_3SCH_3$ | 72 | 1.5 | −288 | 7.4 |
| THP | −553 | 1.67[a] | −357 | |
| $CH_3CN$ | −586 | 3.92 | −1967 | 4.4 |

[a] MOPAC 6 (AM1) calculation.

In previous publications[7,8] we demonstrated that the interaction between DABCO in its (2p3s) Rydberg state and rare gases and saturated hydrocarbons is more repulsive (smaller binding energy) than that found for the DABCO ground state and these solvents. This determination is based on the observation of a cluster blue shift for the DABCO (2p3s) ← $(2p)^2$ transition. Similar reasoning can be employed to rationalize the cluster blue shift results presented in the present study for the solvents Kr, $N_2$, $C_2H_4$, cyclohexane, and methylcyclohexane.

Below, we will discuss the behavior of the other solvents (aromatics and polar systems) and in particular explore the nature of the interaction between excited Rydberg states and polar and polarizable molecules.

**A. Dipole-Induced Dipole Interaction in Rydberg States.** The dipole-induced dipole interaction energy between a dipole and a polarizable sphere depends critically on the orientation of the dipole with respect to the line joining their centers; for maximum interaction energy, the dipolar axis of the solvent should be parallel to this particular radius of the polarizable sphere. From a simple classical treatment, the maximum dipole-induced dipole interaction energy between a polarizable sphere and a dipole can be written as (in units of $cm^{-1}$)[19]

$$V_{did} = (-2.01 \times 10^4)\mu^2(\alpha/r^6) \quad (1)$$

in which $\mu$ is the dipole moment in Debyes, $\alpha$ is the polarizability in $Å^3$, and $r$ is the center to center distance (Å) between the dipole and the sphere. In this instance the DABCO excited (2p3s) Rydberg state is the "polarizable sphere" and the solvent molecule (e.g., $CH_3CN$, $CH_3SCH_3$, etc.) is the orientable dipole. For DABCO/solvent clusters, $r \sim 5.0$ Å and the polarizability of the Rydberg state is estimated to be ~100 $Å^3$ on the basis of experimental results for cyclic ketones.[9] Thus, eq 1 becomes

(18) Li, S.; Bernstein, E. R. *J. Chem. Phys.* **1991**, *95*, 1577.

(19) Atkins, P. W. *Physical Chemistry*, 2nd ed.; W. H. Freeman & Co.: San Francisco, 1989.

$$V_{did} = -128\mu^2 \quad (2)$$

Solvent dipole moments are given in Table II[20] and can be used directly in this expression. Equation 2 gives the maximum value for the dipole-induced dipole interaction for DABCO/solvent clusters in the (2p3s) Rydberg state. The DABCO/solvent interaction for the ground-state cluster would be expected to be about a factor of 100 smaller, since $\alpha$ (ground state) is approximately a few cubic angstroms.[20]

The interaction between DABCO and polar solvent molecules in the form expressed by eqs 1 and 2 could thus give rise to a red shift in the (2p3s) ← $(2p)^2$ Rydberg transition for clustered DABCO relative to that for the unclustered DABCO. Since in this classical picture all "interaction types" are additive, this red shift would be expected in addition to other "shift mechanisms" active or appropriate for a particular solute/solvent pair. Therefore, the net transition energy shift for a polar solvent cluster must be the sum of all repulsive and attractive interactions appropriate for both the excited Rydberg state and the ground state.

This simple treatment can be employed to interpret the spectroscopic shift for DABCO$(CH_3SCH_3)_1$. The $CH_3SCH_3$ dipole moment is 1.5 D (Table II), and the calculated maximum dipole-induced dipole shift for this system is, according to eq 2, $-288$ cm$^{-1}$. The experimental shift for DABCO$(CH_3SCH_3)_1$ is $+72$ cm$^{-1}$ for the major cluster geometry observed. The repulsive interaction expected in addition to this attractive one can be estimated by considering the DABCO$(CH_3CH_2CH_3)_1$ cluster, whose transition blue shift is 267 cm$^{-1}$.[8] The net transition shift is then estimated to be $-21$ cm$^{-1}$. The greatly reduced blue shift for the DABCO$(CH_3SCH_3)_1$ Rydberg transition with respect to that for DABCO$(CH_3CH_2CH_3)_1$ is explained by this model if one assumes that the repulsive interactions in the Rydberg state of these two clusters are comparable. The geometries for DABCO$(CH_3CH_2CH_3)_1$,[8] $(CH_3OCH_3)_1$ (Figure 1), and $(CH_3SCH_3)_1$ are all very similar and suggest that the dipole-induced dipole interaction is near its maximum allowed value in these systems.

The shift of the Rydberg transition of the DABCO$(CH_3CN)_1$ cluster can be similarly understood. The red shift for this system is nearly 590 cm$^{-1}$ (Table I and Figure 7), and the dipole moment of acetonitrile is 3.9 D (Table II). According to eq 2, this system can have a dipole-induced dipole interaction of up to $V_{did} \sim 1950$ cm$^{-1}$. Figure 1 shows that the equilibrium geometry for the ground state of this cluster is not favorable for this maximum interaction, and thus a reduced cluster red shift is not unreasonable. Additionally, the excited-state equilibrium geometry might well be different from that of the ground state, such that the dipole-induced dipole interaction would be closer to its maximum value for the excited-state cluster. The orientation of the $CH_3CN$ solvent molecule dipole axis would then be parallel to the $C_3$ DABCO axis. This cluster geometry change upon (2p3s) ← $(2p)^2$ DABCO excitation would also account for the width of the DABCO$(CH_3CN)_1$ cluster spectrum (Figure 7); the width is attributed to the relative shift of the equilibrium energy minima of the two potential surfaces and the concomitant high density of vibrational states for the Franck–Condon accessible portion of the upper surface.

Induced dipole-induced interactions can also be considered as a source for these spectroscopic shifts, but as can be seen from Table II, the shifts do not scale with solvent polarizability. This point is discussed more thoroughly in refs 8 and 17.

The spectral shifts for DABCO$(CH_3SCH_3)_1$ and $(CH_3CN)_1$ Rydberg transitions can thus be qualitatively understood on the basis of the above dipole-induced dipole and repulsive interactions in the Rydberg state. These results suggest that both of these interactions play an important role in the interaction between a Rydberg state and its environment. The simple classical treatment of the dipole-induced dipole interaction suggests that it is proportional to the square of the solvent dipole moment and that it depends on the orientation of the solvent dipole axis with respect to the $C_3$ axis of DABCO.

**B. Electron Delocalization over the Solvent: Electron-Transfer Interaction.** The above discussion of section IVA notwithstanding, a comparison of the spectroscopic shifts for DABCO clustered with amine, ether, and aromatic solvent molecules reveals that the dipole-induced dipole interaction alone cannot account for the experimentally observed cluster red shifts (Figures 2, 3, 5 and Table I). The DABCO clusters with nonpolar benzene, dioxane, and DABCO, and with slightly polar toluene ($\mu = 0.39$ D), display very large red shifts (see Table I). These large red shifts cannot be associated with a dipole-induced dipole interaction but must arise from another sizable interaction. In addition, the transition origin red shifts for DABCO clustered with amines ($NH_3$, TEA, DABCO) display an inverse correlation with solvent dipole moment (Figure 2). Therefore, a special interaction must occur between the 3s Rydberg state of DABCO and amine, ether, and aromatic molecules.

A number of "special" interaction mechanisms have been proposed to account for the apparent formation of amine Rydberg-state excimers or exciplexes in solution. These mechanisms include the following: (1) an ion–dipole interaction between the 3s Rydberg molecule cationic core and a polar solvent[21,22] and (2) a "three-electron $\sigma$-bond" between the 2p lone pair electrons of the solvent and the singly occupied 2p orbital of the excited solute.[23] Neither of these can apply here because the aforementioned dipole moment/shift trend and the calculated cluster equilibrium geometry display the incorrect characteristic behavior.

In the following discussion we suggest that the attractive interaction between the (2p3s) DABCO Rydberg state and amine, ether, and aromatic solvents arises from an electron- or charge-transfer interaction between the two molecules. The 3s Rydberg electron is delocalized into the available, spatially and energetically similar, empty solvent orbital. This delocalization or electron-transfer interaction generates a strong interaction between the (2p3s) excited DABCO molecule and the solvent molecule. If the solvent 3s orbital is not close in energy to the DABCO 3s orbital, this interaction is not significant. The interaction between the (2p3s) excited DABCO and a saturated hydrocarbon solvent, for example, is not large because the available 3s orbital in these solvents is at a much higher energy. An excellent example of such an interaction is found in the argon dimer. The ground-state $Ar_2$ is bound by 93 cm$^{-1}$, while the 4s excited state is bound by $\sim$5000 cm$^{-1}$.[24] Thus, Rydberg states can have a very large attractive intermolecular interaction through a charge- or electron-transfer interaction mechanism.

This attractive interaction for an excited Rydberg state is important or dominant under the following three conditions: (1) the Rydberg orbital is diffuse and has a large spatial extent; (2) the 3s Rydberg orbital is nondirectional; and (3) the accepting empty solvent orbitals are also 3s Rydberg orbitals of nearly the same properties and energy.

A comparison of the 3s orbitals of DABCO, TEA, and $NH_3$ makes this latter point clear. The (2p3s) ← $(2p)^2$ transitions for these molecules lie at 35 786, 42 000, and 46 140 cm$^{-1}$ respectively.[11] The transition energy for DABCO is probably lowered because the two $(2p)^2$ lone pair electrons interact in the ground state.[25] The ABCO (2p3s) ← $(2p)^2$ transition lies at 39 100 cm$^{-1}$. Thus, the 3s orbital energies for these molecules may even be closer than the transition energies would suggest.

(20) Lide, D. R. *Handbook of Chemistry and Physics*, 71st ed.; The Chemical Rubber Co.: Cleveland, OH, 1990–1991.

(21) Halpern, A. M. *J. Phys. Chem.* **1981**, *85*, 1682.
(22) Muto, Y.; Nakato, Y.; Tsubomura, H. *Chem. Phys. Lett.* **1971**, *9*, 597.
(23) Ruggles, C. J.; Halpern, A. M. *J. Am. Chem. Soc.* **1988**, *110*, 5692.
(24) Herman, P. R.; LaRocque, P. E.; Stoicheff, B. P. *J. Chem. Phys.* **1988**, *89*, 4535.
(25) Bischof, P.; Hashmall, J. A.; Heilbronner, E.; Hornung, V. *Tetrahedron Lett.* **1969**, *46*, 4025.

DABCO/ether and aromatic solvent cluster shifts are also large. The electron-transfer interaction mechanism applies to these systems, as well. Even though the (2p3s) ← $(2p)^2$ transition of ethers and the $(\pi 3s) \leftarrow (\pi)^2$ transition of aromatics are ca. 50 000 and 60 000 $cm^{-1}$, respectively,[11] the 3s Rydberg states of these solvents are probably close to that of DABCO. The higher transition energies arise from low ground-state $(2p)^2$ and $(\pi)^2$ configuration energies.

The cluster transition shifts for DABCO/amine, ether, and aromatic solvent clusters are thus correlated with the electronic structure of the solvent molecules. The 3s Rydberg states of DABCO and the amine and ether solvents employed in these studies are similar and degenerate. The aromatic solvent 3s orbitals are at higher energy than the DABCO 3s orbital but still interact with it. In this latter instance the $\pi\pi^*$, $\sigma\sigma^*$, and $\pi\sigma^*$ excited states could also play an essential role in the DABCO/aromatic solvent cluster interaction. We will suggest in the following paper[26] that the DABCO/amine and ether solvent clusters upon DABCO (2p3s) ← $(2p)^2$ excitation generate an electron-transfer final state, whereas DABCO/aromatic solvent clusters may generate either an energy-transfer or an electron-transfer final state.

Solvent dipole moment induced shifts can also contribute to the observed spectroscopic red shift, as these different contributions should be additive. Table I shows that, for similar systems with and without dipole moments, the solvent with the dipole moment always induces the larger red-shifted cluster transition. Examples of this trend follow for ABCO vs DABCO, dioxane vs THP, and benzene vs toluene.

The large difference in spectroscopic shift between DABCO-$(CH_3OCH_3)_1$ (ca. −460 $cm^{-1}$) and DABCO$(CH_3SCH_3)_1$ (ca. +72 $cm^{-1}$) lends further support to the 3s–3s electron-transfer interaction mechanism. The methyl sulfite first excited Rydberg orbital is 4s, which is much higher in energy than the 3s orbital of $CH_3OCH_3$ and of a different spatial extent and form.

To summarize these points, a Rydberg excited state can have three dominant additional interactions that will distinguish its behavior from that of a valence excited state: (1) repulsion between the diffuse Rydberg electron and the solvent closed-shell electrons, Pauli exclusion principle; (2) an attractive dipole-induced dipole interaction between a polar solvent molecule and the highly polarizable 3s Rydberg excited state of the solute; and (3) 3s Rydberg electron transfer (attractive) to the similar (energy, and spatial extent and overlap) solvent 3s Rydberg orbitals. Relative strengths and importance of the three interactions for solute/solvent properties and Rydberg state behavior depend on solvent electronic properties and polarity. The cluster transition energy shift for the (2p3s) ← $(2p)^2$ solute Rydberg transition reflects the net effect of these various interactions. The above repulsive interaction is the only major additional interaction for Rydberg excited states of DABCO/rare gases, $N_2$, $C_2H_4$, and saturated hydrocarbons. Electron-transfer interactions add to this for solvent systems with low-lying or similar 3s Rydberg orbitals. The dipole-induced dipole interaction becomes important for polar solvents.

**C. Geometry Dependence of Cluster Transition Shifts.** As displayed in Figures 2 and 3 and Table I, more than one cluster geometry is responsible for the spectra of DABCO$(CH_3OCH_3)_1$, $(THP)_1$, and $(TEA)_1$. The transition energy shift is thus critically dependent on cluster geometry. This point was previously made for DABCO$(Ar)_n$ clusters.[7] Shifts can vary for different cluster geometries by as much as a factor of 2 or 3. In this instance of red-shifted cluster transitions, we have assigned the cluster with the most red-shifted transition to the most stable calculated cluster geometry (Figure 1). This assignment derives from the following reasoning: (1) the most stable geometry has the solvent coordinated to the nitrogen end of the DABCO molecule—this geometry has the most overlap between the (2p3s) Rydberg state and the solvent; and (2) this transition (the lowest energy one) is the most intense in the spectra and thus can be associated with the most populated (stable) cluster.

(26) Shang, Q. Y.; Moreno, P. O.; Bernstein, E. R. *J. Am. Chem. Soc.*, following paper in this issue.

## V. Conclusions

The MRES of DABCO clustered with amines (DABCO, ABCO, TEA, $NH_3$), ethers ($CH_3OCH_3$, THP, dioxane), aromatics (benzene, toluene), $CH_3SCH_3$, $CH_3CN$, cyclohexane, methylcyclohexane, Kr, $N_2$, and $C_2H_4$ are obtained and analyzed in this work. The spectra can be understood in terms of cluster transition origins, vibronic transitions involving internal DABCO normal modes, and van der Waals additions built on these features. DABCO/solvent interactions for the (2p3s) Rydberg excited state are probed on the basis of the transition origin shift of the cluster relative to that of the bare DABCO molecule. The differences in transition shift between the various clusters can also be understood. Both positive (blue) and negative (red) shifts for the cluster Rydberg transitions can be observed in the set of clusters investigated. The spectra of DABCO$(Kr)_1$, $(N_2)_1$, $(C_2H_4)_1$, $(cyclohexane)_1$, and $(methylcyclohexane)_1$ show blue shifts for the cluster Rydberg transitions: the blue shift is ascribed to an additional repulsive interaction for the Rydberg state. This interaction arises from repulsion between the electron in a diffuse 3s Rydberg orbital and the solvent closed shells. These solvents have neither dipole moments or available low-lying virtual orbitals. The spectrum of DABCO$(CH_3SCH_3)_1$ shows a small blue shift and that of DABCO$(CH_3CN)_1$ shows a large red shift. Neither of these solvents has available low-lying 3s Rydberg virtual orbitals. The behavior of these clusters is ascribed to an added dipole-induced dipole interaction for the Rydberg state, which both compensates for the above closed-shell repulsive interaction and dominates the shift behavior. This interaction scales with solvent dipole moment and shows the proper orientation dependence predicted for the calculated cluster geometries. The spectra of DABCO/ether and amine clusters show very large (ca. 500 $cm^{-1}$) red shifts. These systems, in addition to the closed-shell repulsion and the (when appropriate) dipole-induced dipole attraction that can occur for (2p3s) Rydberg states, can have an electron-transfer (attractive) interaction in which the 3s Rydberg electron is delocalized into the 3s Rydberg low-lying available orbitals of the solvent. The spectra of DABCO/aromatic solvent clusters also show large red shifts (ca. 350 $cm^{-1}$). A charge-transfer type interaction is appropriate for these clusters, but the resonance and overlap between virtual solvent orbitals and the DABCO 3s orbital is somewhat reduced in this instance compared to that which occurs for the DABCO/amine and ether clusters. Additionally, the excited valence $\pi^*$ and $\sigma^*$ orbitals of the aromatic molecules can interact with the DABCO Rydberg 3s orbital.

All three of these interactions occur for the Rydberg state of DABCO with the appropriate solvents. The most red-shifted transition for a particular cluster can be assigned as the origin of the most stable calculated cluster geometry for that system.

**Acknowledgment.** This work was supported in part by the U.S. Army Research Office.